Silver/Dendrimer Nanocomposites as Biomarkers: Fabrication, Characterization, in Vitro Toxicity, and Intracellular Detection

Wojciech Lesniak,[†,‡,#] Anna U. Bielinska,[†] Kai Sun,[§] Katarzyna W. Janczak,[†] Xiangyang Shi,[†] James R. Baker Jr.,[†] and Lajos P. Balogh*,[†,||,⊥,#]

Center for Biologic Nanotechnology, Microscopy and Image-Analysis Laboratory, Electron Microbeam Analysis Laboratory, Department of Biomedical Engineering, and Macromolecular Science and Engineering, University of Michigan, Ann Arbor, Michigan 48109

Received June 8, 2005; Revised Manuscript Received September 21, 2005

ABSTRACT

We have synthesized water-soluble, biocompatible, fluorescent, and stable silver/dendrimer nanocomposites that exhibit a potential for in vitro cell labeling. Amino-, hydroxyl-, and carboxyl-terminated ethylenediamine core generation 5 poly(amidoamine) dendrimers were utilized to prepare aqueous silver(I)–dendrimer complexes (with the molar ratio of 25 Ag^+ per dendrimer) at the biologic pH of 7.4. Conversion of silver(I)–dendrimer complexes into dendrimer nanocomposites was achieved by irradiating the solutions with UV light to reduce the bound Ag^+ cations to zerovalent Ag^0 atoms, which were simultaneously trapped in the dendrimer network, resulting in the formation of $\{(Ag^0)_{25}$–$PAMAM\_E5.NH_2\}$, $\{(Ag^0)_{25}$–$PAMAM\_E5.NGly\}$, and $\{(Ag^0)_{25}$–$PAMAM\_E5.NSAH\}$ dendrimer nanocomposites (DNC), respectively. The silver–DNCs were characterized by means of UV–vis, fluorescence spectroscopy, dynamic light-scattering, zeta potential measurements, high-resolution transmission electron microscopy, X-ray energy dispersive spectroscopy, and selected area electron diffraction. The cytotoxicity of dendrimers and related silver nanocomposites was evaluated using an XTT colorimetric assay of cellular viability. The cellular uptake of nanoparticles was examined by transmission electron and confocal microscopy. Results indicate that $\{(Ag^0)_{25}$–$PAMAM\_E5.NH_2\}$, $\{(Ag^{0-})_{25}$–$PAMAM\_E5.NGly\}$, and $\{(Ag^0)_{25}$–$PAMAM\_E5.NSAH\}$ form primarily single particles with diameters between 3 and 7 nm. The dendrimer nanocomposites are fluorescent, and their surface charge, cellular internalization, toxicity, and cell labeling capabilities are determined by the surface functionalities of dendrimer templates. The $\{(Ag^0)_{25}$–$PAMAM\_E5.NH_2\}$ and $\{(Ag^0)_{25}$–$PAMAM\_E5.NSAH\}$ nanocomposites exhibit potential application as cell biomarkers.

Introduction. Nanomaterials that can be used in biological systems are required to be water soluble and biocompatible. These materials gained increasing attention in the past few decades because of their unique properties including multiphoton absorption patterning, fluorescence imaging, optical limiting, and nonlinear optical effects that provide outstanding opportunities for application in photonics, biology, and medicine. Poly(amidoamine) (PAMAM) dendrimers hold great promise as templates for metal composite nanoparticles because of their low toxicity and highly regular, branched, three-dimensional structure allowing them to host inorganic

nanoclusters and form stable dendrimer complexes and nanocomposites.[1–20] Dendrimer nanocomposites (DNC) are nanometer-size inorganic/organic hybrid composite particles containing topologically trapped guest atoms/molecules/nanodomains immobilized by dendritic polymer hosts of well-defined size, charge, and terminal functionality.[1–7]

Control of nanoparticle composition and morphology plays an essential role in their future applications. For example, noble metal nanoparticles demonstrate a strong, discrete emission quantum yield that is comparable to bright organic fluorophores used in biological imaging.[8–10] Fabrication of metal/dendrimer nanocomposites by reactive encapsulation requires two steps: (1) binding of metal ions to template dendrimer molecules to form complexes and (2) immobilization of the preorganized metal ions to form nanoclusters with dendrimer templates. The properties of metal–dendrimer nanocomposites also depend strongly on composition, size, and structure.[11–14] It must also be pointed out that the

* Corresponding author. Tel: 716-845-3886; fax: 716-845-8254; e-mail: lajos.balogh@roswellpark.org.
† Center for Biologic Nanotechnology.
‡ Microscopy and Image-Analysis Laboratory.
§ Electron Microbeam Analysis Laboratory.
|| Department of Biomedical Engineering.
⊥ Macromolecular Science and Engineering.
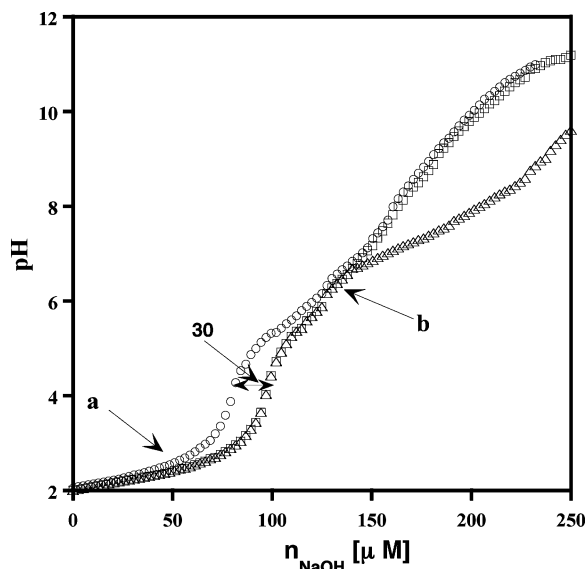# Present address: Roswell Park Cancer Institute, Elm and Carlton Streets, Buffalo, NY 14263.

Figure 1. Potentiometric titration curves of PAMAM_E5.NH$_2$ (circles), Ag$^+$−PAMAM_E5.NH$_2$ 30:1 (squares), and Ag$^+$−PAMAM_E5.NH$_2$ 45:1 systems (triangles). Titrations were performed at room temperature under nitrogen atmosphere for a dendrimer concentration of 3.7×10^{-5} M.

Table 1. UV−vis Spectroscopic Parameters of the Silver/Dendrimer Composite Nanoparticles

material	wavelength (nm)	absorbance
[(Ag$^+$)$_{25}$−PAMAM_E5.NH$_2$]	285 and 416	1.95 and 0.2
[(Ag$^+$)$_{25}$−PAMAM_E5.NGly]	285 and 416	1.05 and 0.1
[(Ag$^+$)$_{25}$−PAMAM_E5.NSAH]	285 and 416	0.7 and 0.72

composition and morphology of dendrimer nanocomposites depend on many factors such as chemical structure, uniformity, and concentration of the template molecules, generation, the metal/template molar ratio, pH, and temperature.[12,15]

The purpose of this article is to describe the synthesis and characterization of silver/dendrimer nanocomposites carrying various surface functionalities and their use as potential cell labels in in vitro experiments. We have developed a novel approach for the controlled fabrication of silver/dendrimer nanocomposites at biologic pH values that includes monitoring of the chelation of Ag$^+$ ions by dendrimer molecules and allows estimation of both their binding capacity and reduction of bound metal ions at desired pH value.

Figure 1 presents the potentiometric titration curves of the PAMAM_E5.NH$_2$ dendrimer and its Ag$^+$ complexes at two different silver-to-dendrimer molar ratios (Ag$^+$/D = 30:1 and Ag$^+$/D = 45:1). Complexation of Ag$^+$ to the PAMAM_E5.NH$_2$ dendrimer induces deprotonation of the nitrogen binding sites, which is reflected in the different shape of the curves related to titration of the dendrimer in the absence (circles) and presence (squares and triangles) of silver ions. At Ag$^+$/D = 30:1 molar ratio, no precipitation was observed over the investigated pH range, indicating that silver ions were completely bound to the dendrimer. Comparison of both titration curves reveals that binding of Ag$^+$ ions to PAMAM_E5.NH$_2$ occurs in the pH range of 2.8−7 (marked in the graph as range a−b). As indicated in the graph, equivalent amounts of H$^+$ ions were released during this process. At Ag$^+$/D = 30:1 and above pH = 7, both curves were similar, suggesting stable species. On the contrary, in the Ag$^+$−PAMAM_E5.NH$_2$ 45:1 system, precipitation of silver hydroxide was observed. The hydrolysis of unbound Ag$^+$ ions starts around pH 7.5, which is evidently visible from the titration curve associated with this sample (triangles) and in agreement with the solubility constant of Ag(OH) ($-\log(K_{sp})$) = 7.59). To our knowledge, this is the first demonstration of the successful application of potentiometry for monitoring metal ion binding to PAMAM dendrimers and estimation of their binding capacity toward metal ions. Unfortunately, the stability constants of silver−PAMAM_E5.NH$_2$ cannot be estimated based on conventional theory because the complexation of metal ions to PAMAM dendrimers occurs in a nonstoichiometric manner due to both the high number of binding sites within the dendrimer and the many possible overlapping equilibrium processes.[16] Moreover, Young at al[17] and Briber at al[18] have shown that changing the pH of a dendrimer solution results in a corresponding change of the structure of dendrimers that can accommodate the dense shell and dense core conformation in acidic and basic pH, respectively. Muthukumar and co-workers have further demonstrated that a reversible transition between these two structures may be observed and that intermolecular density profile of dendrimers depends on pH.[19] All of these factors should be considered for the evaluation of stability constants of metal/dendrimer complexes.

Potentiometric data obtained for the Ag$^+$−PAMAM_E5.NH$_2$ system was applied to design the synthesis

Table 2. Summary of Dynamic Light-Scattering and Average Zeta Potential Data of {(Ag^0)$_{25}$−PAMAM_E5.NH$_2$}, {(Ag^0)$_{25}$−PAMAM_E5.NGly}, and {(Ag^0)$_{25}$−PAMAM_E5.NSAH} Nanocomposites Obtained for 1 mg/mL Aqueous Samples at pH 7.4

material	number weighting mean diam (nm)	volume weighting mean diam (nm)	intensity weighting mean diam (nm)	zeta potential (mV)
{(Ag^0)$_{25}$E5.NH$_2$}	10.8 (99.6%) ± 0.8 37.8 (0.4%) ± 2.3	11.1(83.7%) ± 1 38.7(15.5%) ± 3.3 149 (0.8%) ± 18.6	11.3 (4%) ± 1 40.5 (29.9%) ± 3.8 154.6 (66.1%) ± 17.5	+19.45
{(Ag^0)$_{25}$E5.NGly}	11.5 (100%) ± 1.6	12.2 (94.8%) ± 1.5 107.5 (5.2%) ± 12.2	12.8 (2.9%) ± 1.3 111.8 (97.1%) ± 15.2	+5.93
{(Ag^0)$_{25}$E5.NSAH}	10.9 (96) ± 0.8 27.1 (4%) ± 3	11.1(55.3%) ± 1.9 28.5 (42.3%) ± 4.3 134.8 (3.7%) ± 14.2	11.4 (1.14%) ± 0.9 29.7 (11.9%) ± 3.5 139.7 (87%) ± 17.5	−18.17

of silver nanoparticles stabilized by PAMAM_E5.NGly and PAMAM_E5.NSAH dendrimers having a comparable number of nitrogen ligands. Comparison of the different terminal groups (i.e., the cationic and strong electron-donor NH_2 with the polar and weak proton-donor glycidol, as well as the anionic carboxyl terminal groups) offers an opportunity to study how template surface properties influence the formation of the composite nanoparticles. For each dendrimer template, the same $Ag^+/D = 25:1$ molar ratio was used. Briefly, $[(Ag^+)_{25}-PAMAM\_E5.NH_2]$, $[(Ag^+)_{25}-PAMAM\_E5.NGly]$, and $[(Ag^+)_{25}-PAMAM\_E5.NSAH]$ complexes were obtained by mixing aqueous solutions of dendrimer templates and Ag^+ ions at room temperature and at pH 2.5. The pH was subsequently increased with NaOH solution to obtain a final dendrimer concentration of 1 mg/mL at pH = 7.4. To avoid chemical contamination, Ag^+ ions in the dendrimer complexes were reduced using UV irradiation. After irradiation, the originally colorless aqueous solutions of $[(Ag^+)_{25}-PAMAM\_E5.NH_2]$, $[(Ag^+)_{25}-PAMAM\_E5.NGly]$, and $[(Ag^+)_{25}-PAMAM\_E5.NSAH]$ complexes became transparent yellow-brown, light-gray, and yellow, respectively, indicating the reduction of Ag^+ to Ag^0 and the formation of $\{(Ag^0)_{25}-PAMAM\_E5.NH_2\}$, $\{(Ag^0)_{25}-PAMAM\_E5.NGly\}$, and $\{(Ag^0)_{25}-PAMAM\_E5.NSAH\}$ nanocomposites. There was no precipitation. Table 1 lists the UV−vis spectroscopic parameters of silver/dendrimer composite nanoparticles (spectra are presented in the Supporting Information). Solutions of silver DNCs exhibit two peaks, one at 285 and another at 416 nm. The signal at 416 nm can be assigned as a plasmon peak resulting from aggregated silver DNC particles. Because of the different surface properties of different dendrimer hosts, the degree of aggregation is clearly different at pH = 7.4 for these composite nanoparticles.[20]

Absorbance peaks at 285 nm might be related to partially oxidized dendrimer molecules formed during photolytic reduction of Ag^+ cations.[21] Because the spectra of the UV-exposed host dendrimers revealed only very low intensity absorbance peaks at 285 nm (see the Supporting Information), this explanation is less likely here, and we assign the 285-nm peaks that originate from single (not associated) silver nanocomposite particles. In Table 1, UV−vis peak values and intensities are compared. Because the silver concentrations in the three nanocomposites are identical, the spectral changes must be due to structural differences. If the relative intensity of the absorbance peaks depends on the ratio between single particles and aggregates, then this difference suggests that the $\{(Ag^0)_{25}-PAMAM\_E5.NSAH\}$ nanocomposite is more significantly aggregated under the experimental conditions used than $\{(Ag^0)_{25}-PAMAM\_E5.NH_2\}$ and $\{(Ag^0)_{25}-PAMAM\_E5.NGly\}$. From dynamic light-scattering measurements, we found that by number average each sample is dominantly composed of single small particles. However, the size distribution and surface charge of the nanocomposite particles were determined by the terminal groups of the dendrimer hosts (Table 2). $\{(Ag^0)_{25}-PAMAM\_E5.NH_2\}$ and $\{(Ag^0)_{25}-PAMAM\_E5.NGly\}$ nanocomposites are positively charged because of the partially protonated amino groups of the dendrimer hosts at pH 7.4.

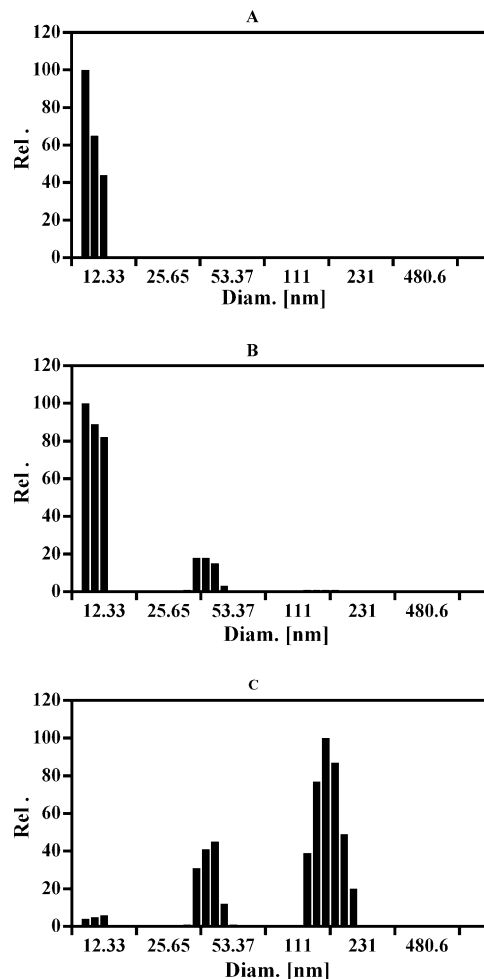**Figure 2.** NICOMP size distribution profiles of the $\{(Ag^0)_{25}-PAMAM\_E5.NH_2\}$ nanocomposite based on dynamic light-scattering measurements. (A) Number weighting (related to the size of nanocomposite particles); (B) volume weighting (related to the concentration of nanocomposite particles); and (C) intensity weighting (related to the interaction of nanocomposite particles with light). Measured in aqueous samples at a dendrimer concentration of 1 mg/mL and pH 7.4

As expected, $\{(Ag^0)_{25}-PAMAM\_E5.SAH\}$ nanocomposite particles carry a net negative charge because the majority of carboxyl groups is deprotonated at pH 7.4. The negatively charged composite nanoparticles displayed a stronger tendency to form higher order aggregates, which explains the relatively high intensity of the absorbance at 416 nm in its UV−vis spectrum.

Figure 2 shows dynamic light-scattering NICOMP size distribution histograms of the $\{(Ag^0)_{25}-PAMAM\_E5.NH_2\}$. Figure 2 demonstrates that the system is composed of primary particles, their clusters, and respective superclusters (clusters of clusters) in a surprisingly narrow distribution. Data (Table 2 and Figure 2) also indicate that the size distribution of the silver DNCs depends on how the measured data are weighted: by numbers, by volume, or by scattering intensity. Comparison of Figure 2A−C reveals that although $\{(Ag^0)_{25}-PAMAM\_E5.NH_2\}$ solution contains dominantly small nanocomposites and only a few clusters including a negligible number of superclusters these larger objects intensively scatter light. The net surface of the particles (thus,
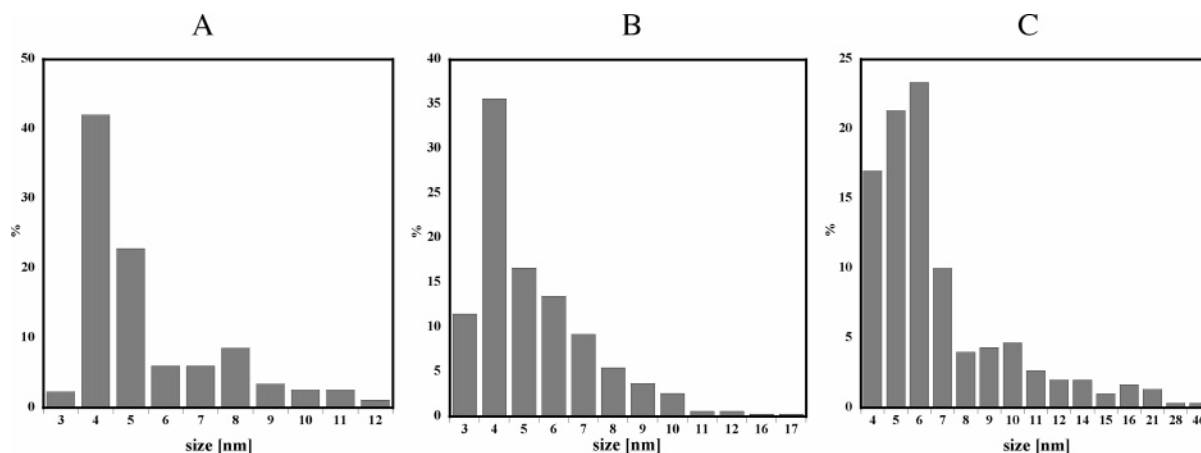
Figure 3. Size distribution profiles of (A) $\{(Ag^0)_{25}-PAMAM\_E5.NH_2\}$; (B) $\{(Ag^0)_{25}-PAMAM\_E5.NGly\}$, and (C) $\{(Ag^0)_{25}-PAMAM\_E5.NSAH\}$ nanoparticles obtained based on TEM images recorded at magnification of 92000x (included in the Supporting Information). Histograms were obtained manually using J-Image computer software.

surface interactions with biologic objects including cells) is governed by the number of particles; relative mass is determined by the volume distribution, but particle visibility will be influenced mostly by the larger aggregates that can efficiently interact with light making them easy to observe. The order of aggregate formation was found to be $\{(Ag^0)_{25}-PAMAM\_E5.NSAH\} > \{(Ag^0)_{25}-PAMAM\_E5.NH_2\} > \{(Ag^0)_{25}-PAMAM\_E5.NGly\}$. The differences in nanoparticle aggregation are explained based on the different intermolecular/interparticle interactions between dendrimer hosts at given pH and temperature. Under the experimental conditions used (pH 7.4), the terminal carboxyl groups of the $\{(Ag^0)_{25}-PAMAM\_E5.NSAH\}$ nanoparticles are partially deprotonated, which promotes dipole−dipole interactions and hydrogen bond formation between the hosts. The $\{(Ag^0)_{25}-PAMAM\_E5.NH_2\}$ DNC is positively charged at this pH, which decreases interparticle interactions and leads to aggregate formation to a lesser extent (these are also mixed structures held together by metal domains that form during composite synthesis[12]). The net surface charge of the PAMAM_E5.NGly dendrimer is close to neutral at pH 7.4 (as shown by the zeta potential data); thus, hydrogen bonding is significantly diminished. In addition, the terminal glycidol moieties further limit aggregation because of the increased steric hindrance. As a result, $\{(Ag^0)_{25}-PAMAM\_E5.NGly\}$ displays the narrowest size distribution, predominantly with single particles present in its solution.

Silver DNCs were further analyzed by means of transmission electron microscopy. Figure 3 shows size distribution histograms for the $\{(Ag^0)_{25}-PAMAM\_E5.NH_2\}$, $\{(Ag^0)_{25}-PAMAM\_E5.N.Gly\}$, and $\{(Ag^0)_{25}-PAMAM\_E5.N.SAH\}$ nanoparticles obtained based on evaluation of the low-magnification TEM images (Supporting Information Figure 2s). The size distribution of the investigated silver DNCs depends on the kind of terminal groups of dendrimer templates. The histogram obtained for $\{(Ag^0)_{25}-PAMAM\_E5.NSAH\}$ proves the presence of elevated relative ratios of primary and higher order aggregates in this system. Nevertheless, each sample contains predominantly single particles with diameters ranging from 3 to 7 nm. There

is a difference between the size distribution obtained from DLS and TEM imaging, which results from differences between the applied methods. Preparation of the samples for TEM requires dilution of the solution of investigated silver DNCs by a factor of 2, followed by evaporation of the solvent under vacuum; the treatment used may influence the observed aggregation degree. DLS measurements are collected in solution, whereas for TEM, dry samples are used that may not reflect the exact particle distribution present in solution. Diameters measured from TEM images are only related to the location of the metallic domains in the nanocomposites without observing the organic host of the metal domains, whereas DLS measurements take into account the whole composite nanoparticle. Finally, because of the resolution threshold of the used particle-sizer (>5 nm), particles with a hydrodynamic radius of 11 nm and smaller can be considered as the same fraction close to the lower limit. Despite the above-described differences, both methods provide evidence that $\{(Ag^0)_{25}-PAMAM\_E5.NSAH\}$ nanoparticles exhibit the highest degree of aggregation that correlates with the relatively high intensity of the absorbance at 416 nm in the UV−vis spectrum related to this system.

HRTEM images taken from arbitrarily selected $\{(Ag^0)_{25}-PAMAM\_E5.NH_2\}_n$ aggregate particles suggest that, in the aggregates, crystalline silver domains may form in time (see the Supporting Information). The lattice images indicate that these particles contain either several single crystals or polycrystalline Ag^0. At this point, it is not clear that the transition to semicrystalline structure occurs in solution or during the HRTEM sample preparation method.

Several silver/dendrimer nanocomposites have been reported to be fluorescent.[9,10] The $\{(Ag^0)_{25}-PAMAM\_E5.NH_2\}$, $\{(Ag^0)_{25}-PAMAM\_E5.NGly\}$, and $\{(Ag^0)_{25}-PAMAM\_E5.NSAH\}$ nanoparticles are also fluorescent and can be excited in wavelengths ranging from 300 to 400 nm, resulting in high-intensity emissions in the range of 400−500 nm (see Supporting Information Figure 4s). Prompted by the fluorescence properties of investigated nanocomposites, we have investigated whether these materials can be used in biologic systems as biomarkers that can be observed by both TEM
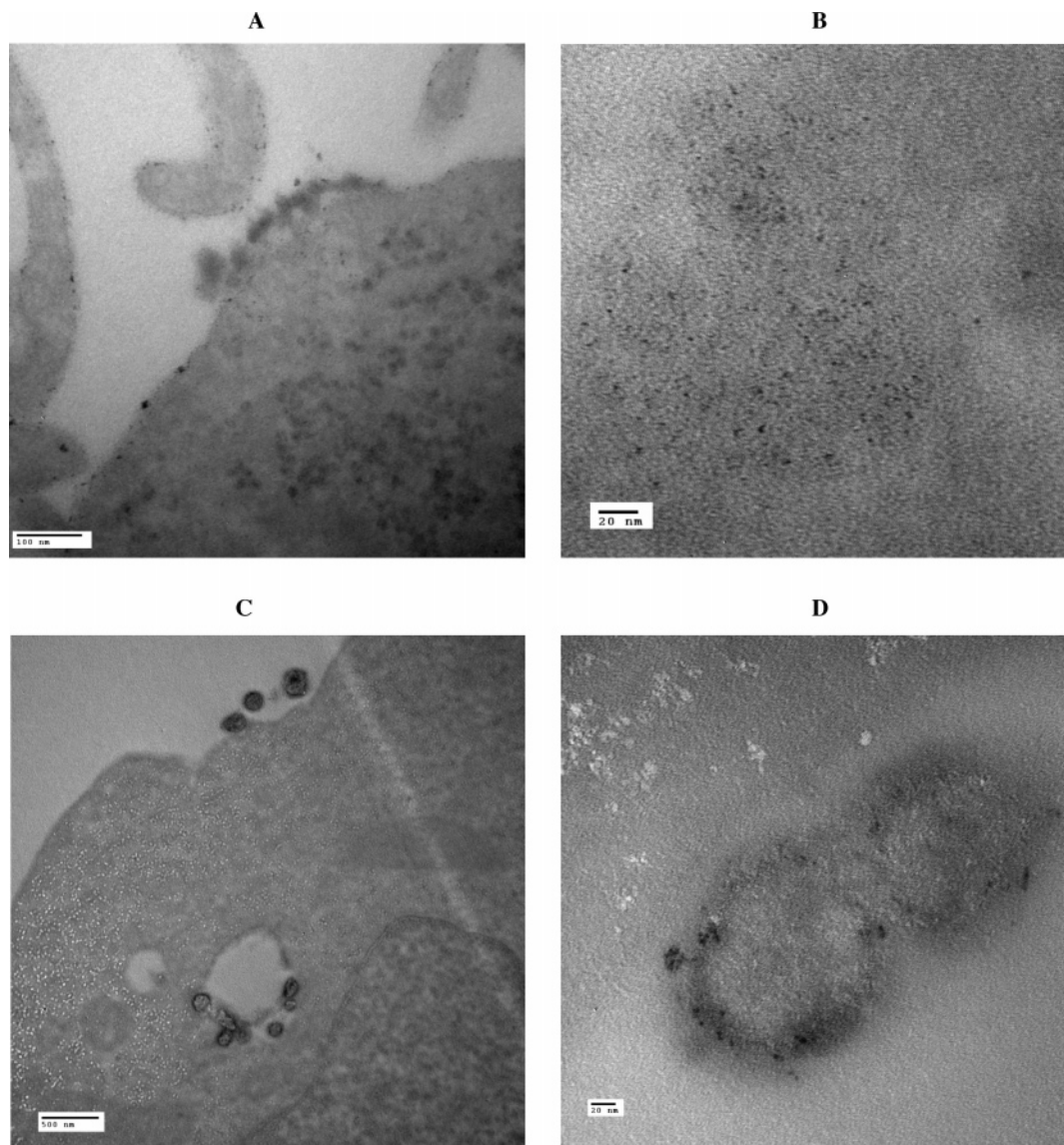
Figure 4. Representative TEM images of NIH3T3 and U937 cell lines incubated with $\{(Ag^0)_{25}-PAMAM\_E5.NH_2\}$ nanoparticles for 1 h at 37 °C and at 500 nM DNC concentration. (A and B) NIH3T3 cell showing DNCs located on the surface of the cell and randomly dispersed single particles in the cytoplasm, respectively; (C and D) U937 cell viewing the agglomerates of DNCs located on the surface of the cell and trapped in the phagocytic or endocytic vesicles.

and fluorescence spectroscopy. As the first step, the cytotoxicity of the PAMAM_E5.NH₂, PAMAM_E5.NGly, and PAMAM_E5.NSAH dendrimer templates and their silver DNCs was examined in KB, Rat2, NIH3T3, and U937 cell cultures using an XTT colorimetric assay of cellular viability. We have found similar toxicity profiles for both the dendrimer hosts and their nanocomposites, suggesting that templates also determine the in vitro toxicity of nanocomposites (Supporting Information Figure 5s). Neither the PAMAM_E5.NGly dendrimer nor the $\{(Ag^0)_{25}-$ PAMAM_E5.NGly} nanocomposite were toxic for KB cells in the concentration range of 0−2 μM. PAMAM_E5.NH₂, PAMAM_E5.NSAH, and their respective silver DNCs exhibited some cytotoxicity above 1 μM concentration. The following order was observed: PAMAM_E5.NH₂, $\approx$ $\{(Ag^0)_{25}-PAMAM\_E5.NH_2\}$ > PAMAM_E5.NSAH, $\approx$ $\{(Ag^0)_{25}-PAMAM\_E5.NSAH\}$ > PAMAM_E5.NGly, $\approx$ $\{(Ag^0)_{25}-PAMAM\_E5.NGly\}$. Similar results were obtained

for Rat2, NIH3T3, and U937 cell lines. As the next step, the cellular uptake of nanocomposites was examined. Because of the high electron density of inorganic domains, the Ag/dendrimer nanocomposite particles can be visualized easily in cells by means of TEM because silver DNC particles exhibit contrasts, sizes, and shapes different from those of cellular organelles. Figure 4 displays representative TEM images collected for NIH3T3 (A and B) and U937 (C and D) cell lines incubated with $\{(Ag^0)_{25}-PAMAM\_E5.NH_2\}$ nanoparticles. After 1 h incubation at 37 °C, {Ag} nanocomposite particles were observed in the form of randomly dispersed single particles or agglomerates on the surface of cellular membranes, in the cytoplasm, or trapped by the phagocytic or endocytic vesicles. It seems that internalization of the polycationic $\{(Ag^0)_{25}-PAMAM\_E5.NH_2\}$ nanoparticles may occur through two distinct mechanisms: both phagocytosis and diffusion via cell walls may take place. Similar results were obtained for the polyanionic $\{(Ag^0)_{25}-$
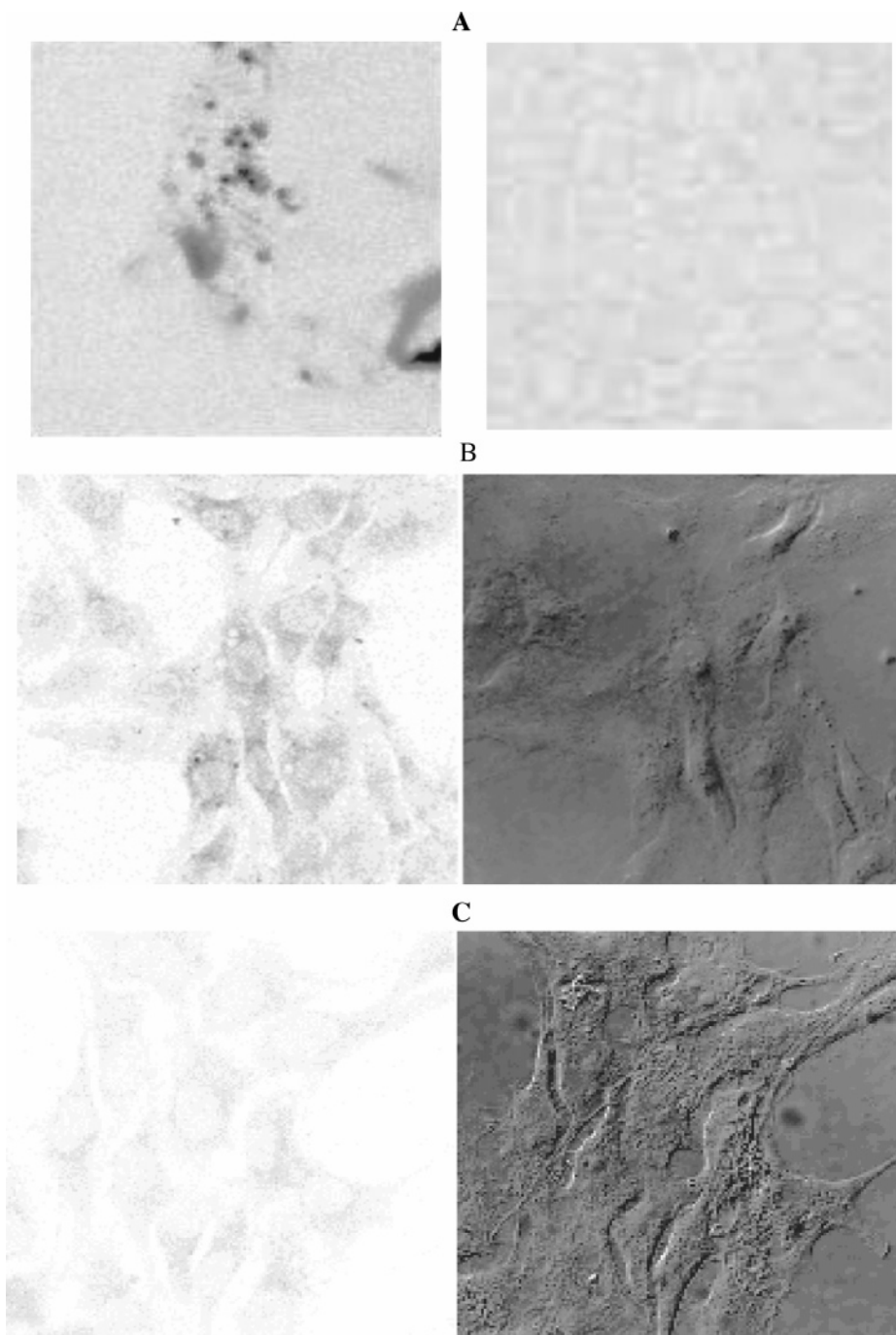
Figure 5. Inverted confocal microscopy images of (A) PAMAM_E5.NH$_2$ (right panel, no fluorescence was detected) and {(Ag^0)$_{25}$−PAMAM_E5.NH$_2$} (left panel, areas exhibiting intense fluorescence can be clearly seen) mixed with the prolong antifade kit; (B) Rat2 cells incubated with {(Ag^0)$_{25}$−PAMAM_E5.NH$_2$} nanocomposite at concentration of 500 nM for 2 h at 37 °C in PBS, pH 7.4, recorded in the fluorescence (left panel) and DIC (right panel) modes; (C) control cells. A significant increase of intracellular fluorescence in cells incubated with {(Ag^0)$_{25}$−PAMAM_E5.NH$_2$} nanocomposite compared to control cells was observed.

PAMAM_E5.NSAH} nanocomposite, whereas cellular uptake of the neutral {(Ag^0)$_{25}$−PAMAM_E5.NGly} was low (data not shown). (Quantitative analysis in this case was not feasible because of the very small size (3−7 nm) of composite nanoparticles compared to cell size.) The cellular uptake and potential application of {(Ag^0)$_{25}$−PAMAM_E5.NH$_2$}, {(Ag^0)$_{25}$−PAMAM_E5.NGly}, and {(Ag^0)$_{25}$−PAMAM_E5.NSAH} DNCs as cell labels was further studied by confocal microscopy. Rat2 cell culture was incubated with either dendrimers or their corresponding silver

DNCs for 2 h at 37 °C in PBS buffer (pH 7.4) at 100, 500, and 1000 nM concentrations (exact conditions are described in the Supporting Information). To test the possibility of using confocal microscopy in order to visualize silver/dendrimer nanocomposites, we placed a drop of aqueous solution of each DNC on microscopy cover glass and mixed it with a prolonged kit. The detection conditions for the confocal instrument were set up based on the fluorescence properties of silver DNCs; thus, scanning was performed using a UV laser operating at 364 nm and a 465−485 nm

emission filter (Figure 5A, inverted image). The nanocomposite containing samples but not dendrimer template exhibited regions of relatively strong fluorescence. Similar results were obtained for PAMAM_E5.SAH, $\{(Ag^0)_{25}-$PAMAM_E5.NSAH$\}$, and PAMAM_E5.NGly, $\{(Ag^0)_{25}-$PAMAM_E5.NGly$\}$ materials (data not shown). Figure 5B and C displays inverted fluorescence (left panels) and DIC (right panels) images of Rat2 cells incubated with 500 nM of $\{(Ag^0)_{25}-$PAMAM_E5.NH$_2\}$ nanocomposite and a control sample, respectively. Both sets were collected under the same experimental conditions (the values of PMT and gain power were set to low to minimize the autofluorescence of cells). Cells incubated with $\{(Ag^0)_{25}-$PAMAM_E5.NH$_2\}$ exhibited a measurable increase of intracellular fluorescence proving that (a) the fluorescence is not quenched and (b) the nanoparticles were internalized within the cells and visibly located in the cytoplasm. There are also small areas exhibiting relatively strong fluorescence; we speculate that these areas might correspond to the nanocomposite aggregates trapped in the endocytic or phagocytic vesicles, as seen in TEM images. Similar results were obtained for the negatively charged $\{(Ag^0)_{25}-$PAMAM_E5.NSAH$\}$, whereas incubation of Rat2 cells with the nearly neutral $\{(Ag^0)_{25}-$PAMAM_E5.NGly$\}$ nanoparticles did not result in elevated intracellular fluorescence. Overall, the results indicate that the toxicity and uptake of investigated silver DNC correlate with the surface charge of nanoparticles and testing of different cells indicates that the presented behavior of silver DNCs is not limited to specific cell lines. The results presented for silver/dendrimer nanocomposites are in good agreement with similar studies carried out with dendrimers that are used as hosts in this study. For example, positively charged (primary amine terminated) generation 5 PAMAM dendrimers decreased the integrity of the cell membrane and induced the release of the cytoplasmic proteins lactate dehydrogenase (LDH) and luciferase (Luc).[22] In contrast, the acetamide-terminated generation 5 PAMAM dendrimer was shown to have little effect on membrane integrity because of its close-to-neutral net surface charge. It is the first time that in vitro data related to DNCs indicated that biological properties of nanocomposites may be determined by the dendrimer hosts and encapsulation of silver by dendrimer templates does not effect their cytotoxicity.

In summary, we have demonstrated that potentiometric titration is an appropriate tool for controlling metal ion binding to PAMAM dendrimers and to estimate the binding capacity of these polymers at given pH values. Irradiation of the aqueous silver ion/dendrimer complex solutions (pH $= 7.4$) led to the formation of fluorescent, biocompatible, and stable $\{Ag^0\}$ dendrimer nanocomposite particles. $\{(Ag^0)_{25}-$PAMAM_E5.NH$_2\}$, $\{(Ag^0)_{25}-$PAMAM_E5.NGly$\}$, and $\{(Ag^0)_{25}-$PAMAM_E5.NSAH$\}$ formed primarily single particles under our experimental conditions with diameters ranging from 3 to 7 nm. These particles displayed $+19.45$, $+5.93$, and -18.17 mV zeta potential in 1 mg/mL aqueous solution, respectively. The silver DNCs were used for in vitro cell labeling in various cell lines. Biocompatibility tests indicated that level of cytotoxicity of the $\{Ag^0\}$ dendrimer

nanocomposites is similar to that of the host dendrimers and depends on the concentration as well as on the sign and value of the net surface charge. PAMAM_E5.NH$_2$, PAMAM_E5.NSAH dendrimers, and corresponding silver DNCs exhibited cytotoxicity only at relatively high concentrations (around 1 μM), whereas PAMAM_E5.NGly and $\{(Ag^0)_{25}-$PAMAM_E5.NGly$\}$ did not show toxic effects on cells within the applied range ($0-2000\mu$M). $\{(Ag^0)_{25}-$PAMAM_E5.NGly$\}$ could not be observed in the cells by confocal microscopy, probably because of the lack of internalization. However, cells incubated with $\{(Ag^0)_{25}-$PAMAM_E5.NH$_2\}$ and $\{(Ag°)_{25}-$PAMAM_E5.NSAH$\}$ nanocomposites exhibited measurable intracellular fluorescence, in good agreement with the results obtained from TEM. Use of a variety of cell lines for in vitro studies indicated that the described biological properties of silver DNCs could be related to different cell populations. The results presented here suggest biocompatibility and possible applications of dendrimer nanocomposites as stable and unique biologic labels. Preliminary results of amine-terminated nanocomposites have been presented at the MRS 2004 Fall meeting and are available at www.mrs.org.

Abbreviations

PAMAM_E5.NH$_2$: amine-terminated, ethylenediamine core generation 5 poly(amidoamine) dendrimer
PAMAM_E5.NSAH: succinamic acid derivative of PAMAM_E5.NH$_2$ dendrimer
PAMAM_E5.NGly: glycidol derivative of PAMAM_E5.NH$_2$ dendrimer
$[(Ag^+)_{25}-$PAMAM_E5.NH$_2]$ and $\{(Ag^0)_{25}-$PAMAM_E5.NH$_2\}$: silver complex and silver nanocomposite of PAMAM_E5.NH$_2$ dendrimer containing twenty-five silver per dendrimer
$[(Ag^+)_{25}-$PAMAM_E5.NGly$]$ and $\{(Ag^0)_{25}-$PAMAM_E5.NGly$\}$: silver complex and silver nanocomposite of PAMAM_E5.NGly dendrimer
$[(Ag^+)_{25}-$PAMAM_E5.NSAH$]$ and $\{(Ag^0)_{25}-$PAMAM_E5.NSAH$\}$: silver complex and silver nanocomposite of PAMAM_E5.NSAH dendrimer
DNC: dendrimer nanocomposite
DLS: dynamic light-scattering
HRTEM: high-resolution transmission electron microscopy
EDS: X-ray energy dispersive spectroscopy
SAED: selected area electron diffraction
DIC: differential interference contrast

Supporting Information Available: Materials and methods. This material is available free of charge via the Internet at http://pubs.acs.org.

References

(1) Balogh, L.; Swanson, D. R.; Spindler, R.; Tomalia, D. A. *Proc. ACS PMSE,* **1997**, *77*, 118.
(2) Beck Tan, N.; Balogh, L.; Trevino, S. *Proc. ACS PMSE* **1997,** *77*, 120.
(3) Zhao, M.; Sun, L.; Crooks, R. M. *J. Am. Chem. Soc.* **1998**, *120*, 4877.
(4) Balogh, L.; Tomalia, D. A. *J. Am. Chem. Soc.,* **1998**, *120,* 7355.

(5) Esumi, K.; Suzuki, A.; Aihara, N.; Usui, K.; Torigoe, K. *Langmuir* **1998**, *14*, 3157.

(6) Sooklal, K.; Hanus, L. H.; Ploehn, H. J.; Murphy, C. J. *Adv. Mater. A* **1998**, *10*, 1083.

(7) Tomalia, D. A.; Balogh, L. US Patent 6,664, 315B2, December 16, 2003.

(8) Zheng, J.; Dickson, R. M. *J. Am. Chem. Soc.* **2004**, *124*, 13982.

(9) Peyser, L. A.; Vinson, A. E.; Bartko, A. P.; Dickson, R. M. *Science* **2001**, *291*, 103.

(10) Mostafa, A.; El-Sayed, M. A. *Acc. Chem. Res.* **2004**, *37*, 326.

(11) Fevre, P.; Magnan, L. H.; Midoir, A.; Chandesris, D.; Jaffres, H.; Fert, A. R.; Peyrade, J. P. *Surf. Rev. Lett.* **1999**, *6*, 753.

(12) Balogh, L.; Valluzzi, R.; Hagnauer, G. L.; Laverdure, K. S.; Gido, S. P.; Tomalia, D. A. *J. Nanopart. Res*. **1999**, *1*, 353.

(13) Peyser, L. A.; Lee, T. H.; Dickson, R. M. *J. Phys. Chem. B* **2002**, *106*, 7725.

(14) Ottaviani, M. F.; Valluzzi, R.; Balogh, L. *Macromolecules* **2002**, *35*, 5105.

(15) Zheng, J.; Stevenson, M. S.; Hikida, R. S.; Van Patten, P. G. *J. Phys. Chem. B*. **2002**, *106*, 1252.

(16) Diallo, M. S.; Christie, S.; Swaminathan, P.; Balogh, L.; Shi, X.; Um, W.; Papelis, C.; Goddard, W. A., III; Johnson, J. H., Jr. *Langmuir* **2004**, 20, 2640−2651.

(17) Young, J. K.; Baker, G. R.; Newkome, G. R.; Morris, K. F.; Johnson, C. S. *Macromolecules* **1994**, *27*, 3464.

(18) Briber, R.; Bauer, B.; Hammouda, B.; Tomalia, D. *Polym. Mater. Sci. Eng.* **1992**, *67*, 430.

(19) Welch, P.; Muthukumar, M. *Macromolecules* **1998**, *31*, 5892.

(20) Balogh, L.; Laverdure, K. S.; Gido, S. P.; Mott, A. G., Miller, M. J.; Ketchel, B. P.; Tomalia, D. A. *Mater. Res. Soc. Symp. Proc.* **1999**, *576*, 69.

(21) Lee, W.; Bae, Y.; Bard, A. J. *J. Am. Chem. Soc.* **2004**, *126*, 8358.

(22) Hong, S.; Bielinska, A. U.; Mecke, A.; Keszler, B.; Beals, J. L.; Shi, X.; Balogh, L.; Orr, B. G.; Baker, J. R., Jr.; Banaszak Holl, M. M. *Bioconjugate Chem.* **2004**, *15*, 774.

NL051077U